ACS APPLIED MATERIALS & INTERFACES

Research Article

www.acsami.org

Efficient Visible Light Photocatalyst Fabricated by Depositing Plasmonic Ag Nanoparticles on Conductive Polymer-Protected Si Nanowire Arrays for Photoelectrochemical Hydrogen Generation

Chunyang Duan,[∥,†,§] Hui Wang,[∥,†] Xuemei Ou,[†] Fan Li,[†] and Xiaohong Zhang*[,†,‡]

[†]Nano-organic Photoelectronic Laboratory and Key Laboratory of Photochemical Conversion and Optoelectronic Materials, Technical Institute of Physics and Chemistry, Chinese Academy of Sciences, Beijing 100190, China

[‡]Functional Nano & Soft Materials Laboratory (FUNSOM), Jiangsu Key Laboratory for Carbon-Based Functional Materials & Devices and Collaborative Innovation Center of Suzhou Nano Science and Technology, Soochow University, Suzhou, Jiangsu 215123, China

[§]Graduate University of the Chinese Academy of Sciences, Beijing 100039, China

Supporting Information

ABSTRACT: Photoelectrochemical (PEC) water splitting to produce H_2 is a renewable method for addressing the worldwide energy consumption increasing and fossil fuels storage shrinking. In order to achieve sustainable PEC H_2 production, the semiconductor electrodes should have good photo-absorption ability, proper band positions, and chemical stability in aqueous condition. Different from the large-band-gap semiconductors such as TiO_2, which can work efficiently under UV light, Si is an narrow-band-gap semiconductor that can efficiently absorb visible light; however, Si is indirect semiconductor and susceptible to photocorrosion in aqueous solution. In this paper, we demonstrate a new strategy of first protecting and then activating to develop a stable visible light photoanode for photoelectrochemical hydrogen production. This AgNPs/PEDOT/SiNW arrays show an encouraging solar-to-chemical energy conversion efficiency of 2.86 % and a pronounced incident photo-to-current conversion efficiency (IPCE) across the whole visible region. Our strategy proposed here contributes to further improvement of corrosion protection and solar energy harvesting for narrow-band-gap semiconductors that employed in visible light photoelectrochemical and photoelectric conversion applications.

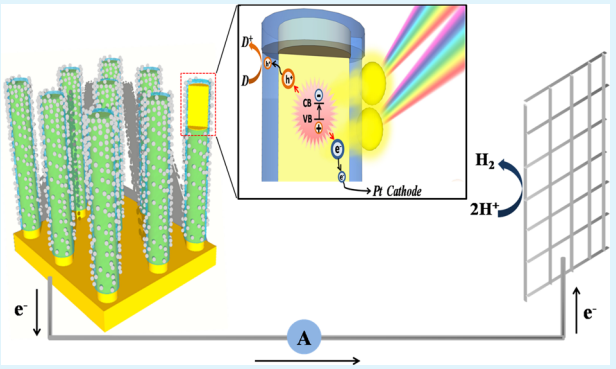

KEYWORDS: *H_2 evolution, photoelectrochemical cell, SiNW array, PEDOT, plasmonic Ag nanoparticles*

INTRODUCTION

Harvesting solar energy and storing it as hydrogen fuel is a sustainable solution for solving the energy crisis and addressing environment problems.[1,2] Since the first presentation by Fujishima and Honda in 1972,[3] splitting of chemicals and water into hydrogen with photoelectrochemical (PEC) cells by the direct use of sunlight has been widely used and intensively studied as a renewable method of solar energy harvesting. A PEC cell uses a semiconductor to absorb solar photons as well as provide electrons and holes, which are then separated by the semiconductor/liquid junction to drive a redox reaction. The reduction reaction that releases H_2 takes place at the cathode, whereas the oxidation reaction takes place at the anode. These two-electrode configurations facilitate the separation of products for widespread solar energy harvesting as well as improve understanding of the photocatalysis mechanism.[4] To date, more than 100 photocatalytic semiconductors have been investigated as photoelectrodes. However, most of these photoactive electrodes are based on metal oxides such as TiO_2,[5] which can work only with UV light because of their large band gaps. UV light accounts for approximately 4% of solar energy, whereas visible light accounts for approximately 43%.[6] Therefore, the development of stable photocatalytic active PEC photoelectrodes that can work with visible light or the entire solar spectrum is highly desirable.[7−9]

The most common method of developing visible light photoelectrodes involves sensitizing wide-band-gap materials (e.g., TiO_2 or ZnO) with sensitizing agents such as dyes and quantum dots,[10,11] or doping them through band gap engineering.[12] Nevertheless, although their photocatalytic activity can been improved, the applications for hydrogen generation are limited by the relatively low efficiency and poor stability of the sensitizing agents.[13] The second strategy involves the direct employment of narrow-band-gap semi-

Received: April 10, 2014
Accepted: May 27, 2014
Published: May 27, 2014

Scheme 1. Schematic Diagram of the Hydrogen Production PEC Cell

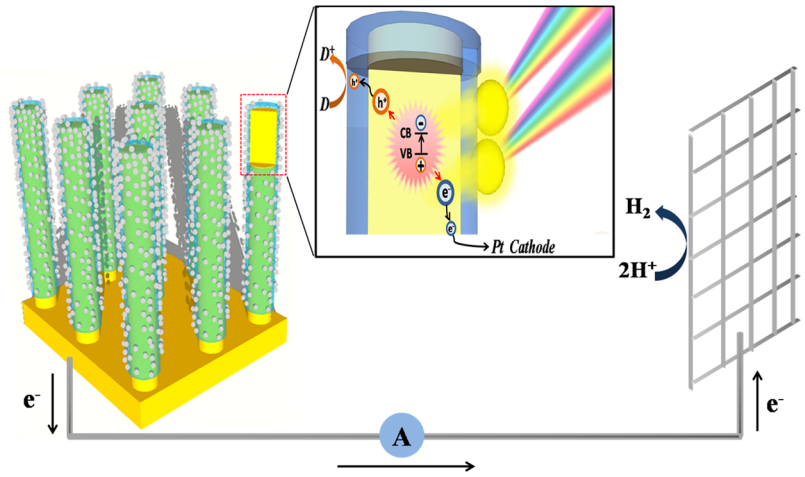

conductors as photoelectrodes, such as α-Fe_2O_3[14−16] and Cu_2O.[17] These semiconductors can efficiently absorb visible light, although their band gaps may be slightly smaller than the energy required for whole water splitting, they still can be used to drive the water splitting after building a tandem PEC for H_2 and O_2 evolution separately via a redox shuttle, such as I^-/IO_3^-, S^{2-}/SO_3^{2-} or Ce^{3+}/Ce^{4+}; namely, the Z-scheme.[18] In addition, these photoanodes are also suitable for using renewable biomass derivatives as electron donors to produce H_2.[19] However, the visible light absorption of these narrow-band-gap semiconductor-based photoelectrodes are still not sufficiently high, and some of them are susceptible to photocorrosion.[20]

In the present work, a new strategy for developing a PEC hydrogen generation photocatalyst with both efficient visible light absorption and chemical stability is reported. This strategy involves coating a robust conductive polymer as a protective layer on the narrow-band-gap semiconductor nanowire (NW) surfaces by electropolymerization, and then enhancing its visible light absorption and photocatalytic efficiency with plasmonic metal nanoparticles (NPs). Although many inorganic materials such TiO_2,[21] C,[22] and organic materials such as, poly-CuTAPc,[23] I:PEDOT,[24] PEDOT:PSS[25] had been applied to stabilizing Si electrode with PVD, CVD, and ALD methods, the important advantages of this proposed strategy are as follows: first, the stable conducting polymer, which can be non-photoactive and transparent, is coated on the electrode surface with a controlled thickness through an electrochemical method. The layer can be so thin that it can isolate the inside NWs from solution thus obtaining good chemical stability, and at the same time, it will not interfere with visible light absorption.[23−25] On the other hand, the polymer layer itself can be durable because it is non-photoactive. Second, owing to its high electronic transport property, the conductive polymer will facilitate the transfer of the minority carriers from the photoelectrode to electrolyte through the electric field at the semiconductor/liquid junction.[25,26] Finally, the conductive polymer protecting layer can increase the effective contact surface between plasmonic metal NPs and semiconductor NWs, thus enhancing visible light absorption. Recently, plasmonic metal NPs (Au and Ag) being used to decorate semiconductors to enhance their visible light harvesting ability have been reported.[27,28] However, directly applying metal NPs on the semiconductor surface may ruin the photocatalytic performance of the system, because the rigid metal NPs deposited on rigid semiconductor surfaces may introduce interface trapping states that can increase electron hole recombination and Fermi level pinning that degrade the photocatalytic activity.[29,30]

Based on the above strategy, a high-performance visible light photoanode was designed by coating a nanoscale layer of poly(3,4-ethylenedioxythiophene) (PEDOT) on the surface of aligned SiNW arrays through electropolymerization, and then, plasmonic AgNPs were decorated on the surface-protected Si/PEDOT core/shell nanowires. PEDOT was selected because it has been shown to have good stability in water and other harsh solvent environments; moreover, its conductivity can reach ∼10 S/cm in its oxidized state.[31,32] In addition, it is reported that a Schottky junction can be formed between the SiNWs and PEDOT, which can facilitate the transfer of photo-generated holes from SiNWs to solution.[25,26]

Silicon, the material used most often for solar energy conversion, has a potential application as a low-cost visible light photocatalyst due to its abundance on Earth and its narrow band gap for visible light absorption. In addition, for solar hydrogen evolution, Si possesses favorable energy band positions, with its conduction band lying 0.45 V negative of the hydrogen evolution potential. Furthermore, SiNWs arrays have light-trapping effects and the special one-dimensional morphology of single NWs can be utilized to shorten the distance of carrier separation, thus enhancing both light absorption and carrier separation efficiency.[33] However, using Si as PEC photoelectrodes for hydrogen generation is challenged due to its low-efficiency indirect band gap transition and its unstable surface in aqueous solutions.[34]

In this study, the enhancement of solar energy harvesting and photocatalytic activity of the AgNPs-modified Si/PEDOT core/shell nanowire array photoanodes (AgNPs/PEDOT/SiNW) were investigated by using Pt mesh as a cathode and a water/methanol system as the electrolyte in a PEC cell (Scheme 1). The PEC cell exhibited a steady photocurrent density of 6.6 mA/cm^2 and a pronounced incident photo-to-current conversion efficiency (IPCE) of ∼35−42% across the visible region from 360 to 870 nm under a 100 mW/cm^2 irradiation with a UV-filtered xenon lamp at zero applied potential (0 V vs SCE); this photocurrent density was observably stronger than when the AgNPs were directly applied to the SiNW photoanode (without PEDOT protecting layer). Hydrogen was effectively produced at a rate of 36.05

dx.doi.org/10.1021/am5021414 | ACS Appl. Mater. Interfaces 2014, 6, 9742−9750

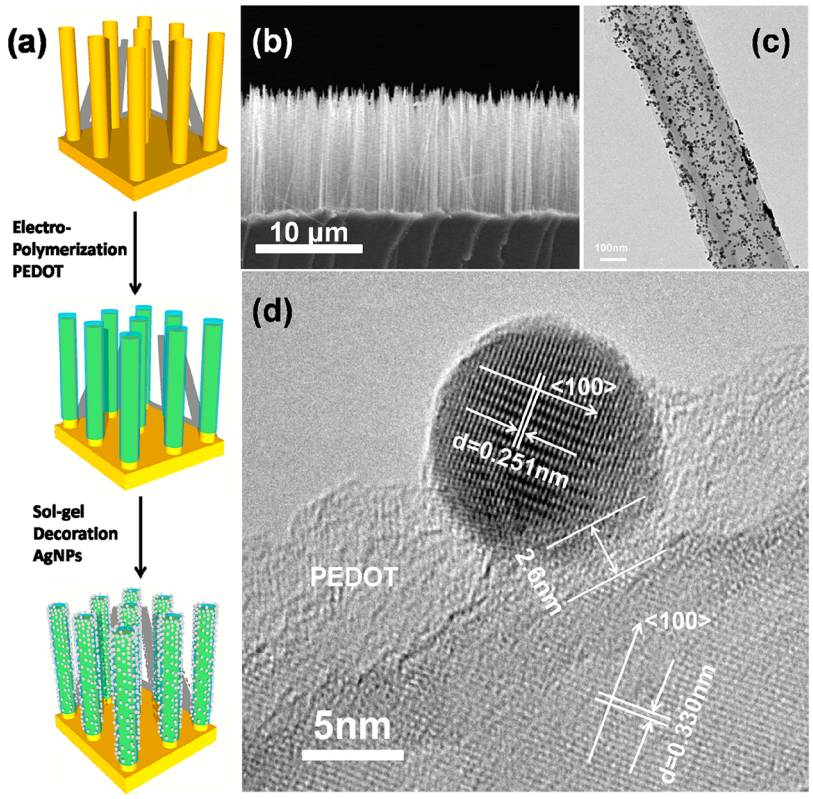

Figure 1. (a) Schematic illustration of the fabrication process of the AgNPs/PEDOT/SiNW arrays. (b) Cross-section SEM image of the AgNPs/PEDOT/SiNW arrays. (c) TEM image of a typical SiNW modified by PEDOT and AgNPs. (d) HRTEM image of the AgNP/PEDOT/SiNW structure.

μmol/(cm^2·h) in a two-electrode system with no external potential applied on the working electrode. The solar-to-chemical energy conversion efficiency of 2.86% produced in this experiment is among the best reported for a stable visible light photoanode for hydrogen generation.[35] The results reveal that the proposed strategy of protecting the narrow-band-gap semiconductor nanostructure with a robust conductive polymer layer and then enhancing its visible light absorption with plasmonic metal NPs is feasible for designing high-performance photoanodes for PEC hydrogen generation.

EXPERIMENTAL SECTION

Synthesis of Silicon Nanowires Arrays. N-type vertical aligned SiNW arrays were prepared via metal-catalyzed electroless etching (MCEE) of n-Si wafer. The commercial heavily doped n-type Si wafers (0.01−0.02 Ω/cm) were cleaned by water and acetone and then immersed in oxidant solution containing H_2SO_4 (97%) and H_2O_2 (35%) (v/v = 3/1) for 10 min (room temperature) to entirely remove organics. The cleaned silicon wafer was immediately immersed into HF−$AgNO_3$ solution in sealed vessels to etch in 50 °C water bath for the designed time, and then immersed into aqua fortis over an hour to remove the residual Ag particles on the wafer. The solution concentrations of HF and $AgNO_3$ were always chosen to be 5 and 0.02 mol/L, respectively.

Synthesis of the AgNPs Decorated Si/PEDOT Core/Shell Nanowires Arrays. SiNWs arrays were washed several times by deionized water and then immersed into 50:1 HF solution for 10 mins and then the H-terminated SiNWs arrays were washed several times by ethanol and acetone. The electro-polymerization and simultaneous deposition of PEDOT on the surface of Si nanowires was performed in a three-electrode cell using 0.01 M 3,4-ethylenedioxythiophene (EDOT) as the monomer in a $LiClO_4$/EtCN electrolyte. The working electrode was the H-terminated SiNWs arrays. A platinum mesh was used as the counter electrode, and a saturated calomel electrode was used as the reference electrode. N_2 was bubbled into the electrolyte for 30 min before electropolymerization and continued during the whole PEDOT deposition process to remove the O_2 from the reaction system. The potential window used for cyclic voltammetric electropolymerization of the PEDOT on the SiNWs electrodes was +1.4 to 0.4 V (vs SCE), at a scan rate of 100 mV/s. Once the electropolymerization was completed, the work electrode was rinsed with EtCN for several times to remove the EDOT monomer and then washed with ethanol to remove the EtCN. Citrate-stabilized AgNPs were decorated onto SiNW arrays by electroless metal deposition method in a solution containing 0.5 mM trisodium citrate and 0.25 mM $AgNO_3$ dissolved in ethanol/water (v/v = 4/1) with NaHB as reducing agent.

Photo-electrochemical Measurement. Photo-electrochemical measurement was conducted using a 500 W xenon lamp as an excitation source. The intensity of the illumination near the surface of the electrode was adjusted to 100 mW/cm^2 with an optical power meter. A CV Instruments 660C potentiostat was used to record steady-state current data. When the experiment was conducted in a three-electrode system, the modified SiNWs arrays were used as working electrode, the platinum mesh was used as the counter electrode and the SCE was used as the reference electrode. Photo-electrochemical measurements were carried out in a water/methanol (v/v = 1/1) mixture (pH = 1, adjusted with H_2SO_4) as electrolyte. When the experiment was conducted in a two electrode system, the counter electrode and the reference electrode were joined together and no external potential was applied to the working electrode.

H_2 Detected by Online Gas Chromatography. Generated H_2 was characterized by GC analysis (14B Shimadzu) using nitrogen as the carrier gas with a molecular sieve column (5 Å; 30 m × 0.53 mm) and a thermal conductivity detector. The retention time of H_2 was ~0.9 min in this detected condition. Firstly, an H_2 calibration curve was obtained using pure H_2. Then, H_2 generated in the photo-electrochemical measurement was injected into the online gas

dx.doi.org/10.1021/am5021414 | ACS Appl. Mater. Interfaces 2014, 6, 9742−9750

chromatography to get the H_2 peak area. Finally, we calculated the real volume of H_2 injected into the 14B Shimadzu, according to the calibration curve.

RESULTS AND DISCUSSION

The fabrication of the novel photoanode AgNP/PEDOT/SiNW arrays is depicted in Figure 1a. Firstly, n-type vertical aligned SiNW arrays were prepared via metal-catalyzed electroless etching (MCEE) of n-Si wafers (Supplementary Information (SI) S1).[36] Then, a PEDOT film was coated on the surfaces of the SiNWs by electro-polymerization (SI S2). The mechanism of electro-polymerization has been reported by Ryosuke Asami et al., and the thickness of the PEDOT film can be controlled on the nanoscale by this method.[37] At last, citrate-stabilized AgNPs were decorated onto SiNW arrays by an electroless metal deposition method in a solution containing 0.5 mM trisodium citrate and 0.25 mM $AgNO_3$ dissolved in ethanol/water (v/v = 4/1) with NaHB as the reducing agent. Figure 1b shows a cross-sectional SEM image of AgNPs/PEDOT/SiNW arrays. The vertically aligned nanowires are ~10 μm in length and stand on the Si substrate. The TEM image of an individual AgNPs/PEDOT/SiNW (Figure 1c) reveals that the NW has an average diameter of 180 nm. The detailed AgNP/PEDOT/SiNW structure can be identified in the high-resolution TEM (HRTEM) image (Figure 1d). The HRTEM image shows that a ~7 nm amorphous thin film is coated to conform on the (100)-oriented crystal SiNW surface, and the diameter of the (100)-oriented crystal AgNP with a hexagonal system is ~10 nm. The formation of the PEDOT layer was also confirmed with infrared (IR) spectroscopy (SI S3).

The absorption spectra of the unmodified SiNW (H-SiNW), PEDOT/SiNW, AgNPs/SiNW (SI S4) and AgNPs/PEDOT/SiNW arrays were measured with a UV/Vis/NIR spectrophotometer equipped with an integrating sphere. The spectra (Figure 2a) have two distinguishing features: first of all, AgNPs/PEDOT/SiNW arrays have the best absorption, and can absorb 45.6% more of light than the unmodified SiNW arrays in the wavelength range from 200 nm to 1000 nm, as calculated through the integrals of the absorption spectrum; secondly, compared to the unmodified SiNW arrays, AgNPs/SiNW arrays exhibit enhanced absorption.

These two features of photo-absorption improvement may be attributed to the AgNPs' surface plasmons that arise from their surface electrons' collective oscillations. It is worth noting, however, that the AgNPs/PEDOT/SiNW arrays exhibit stronger absorption than the AgNPs/SiNW arrays. This result indicates that the nanoscale conformal PEDOT coating can enhance the light absorption. Nevertheless, this result seems counter to the optimized space condition for efficient plasmon resonance, which proposes that a shorter distance between the AgNPs and SiNW can produce stronger plasmon resonance.[38] This contradiction may be due to the fine controlled microstructure of the AgNPs/PEDOT/SiNW system. Although AgNPs and SiNWs were not in direct contact, they were combined with the PEDOT thin layer in an average thickness of about 2–3 nm between them (Figure 1d). This distance does not affect the efficient resonant interaction between AgNPs and SiNW. Furthermore, the soft polymer PEDOT may combine AgNPs and SiNWs with fewer lattice mismatches than would be present in the direct contact approach, resulting in efficient plasmon resonance.

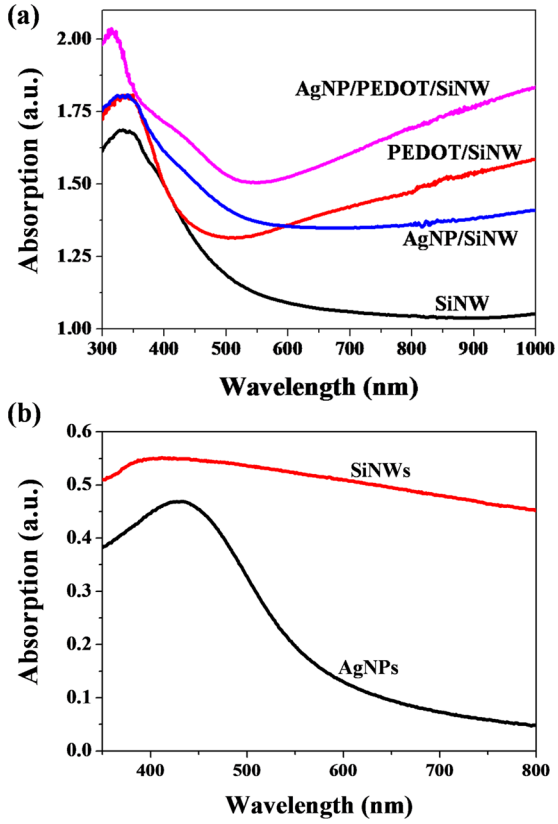

Figure 2. (a) Hemispherical UV–vis absorption spectra of the AgNPs/PEDOT/SiNW arrays, H-SiNW arrays, PEDOT/SiNW arrays, and AgNPs/SiNW arrays. (b) UV–vis absorption spectra of SiNWs and AgNPs dispersed in ethanol.

Furthermore, the plasmon resonance in the AgNPs/PEDOT/SiNW arrays is investigated by comparing the UV–vis absorption spectra of SiNWs and AgNPs in ethonal (Figure 2b). It can be found that the AgNPs have their maximum absorption at 430 nm, which overlapped with the absorption of the SiNWs at 380–430 nm. The overlap indicates that the absorption enhancement of SiNWs through plasmonic resonance is also energetically feasible.[39−41] Meanwhile, it can be seen in Figure 2a that a new shoulder peak centered at 425 nm appeared for the AgNPs/PEDOT/SiNW arrays. This new shoulder absorption peak may be attributed to the absorption resonance between AgNPs and SiNWs.[42]

A PEC cell with the prepared AgNPs/PEDOT/SiNW arrays for use as a photoanode for solar hydrogen generation was fabricated following the designation in Scheme 1 (photoanode area = 0.25 cm^2); a Pt mesh was used as the counter electrode and a saturated calomel electrode (SEC) was used as the reference electrode. The photocurrent and IPCE of the system was measured in a water/methanol (v/v = 1/1) mixture (PH = 1, adjusted with H_2SO_4) under 100 mW cm^{-2} illumination from a xenon lamp. The generated H_2 at the Pt mesh cathode was confirmed by gas chromatography (SI S5).

Figure 3 shows the on–off switching of the PEC photocurrent response at 0 potential bias vs SCE (Figure 3a) and the corresponding I–V curves for all the samples in light and dark (Figure 3b). It reveals that the photocurrent of the unmodified SiNW arrays and AgNPs/SiNW arrays decreased rapidly with irradiation. Their initial photocurrent of ~1.65 mA/cm^2 and ~3 mA/cm^2 both decayed quickly to 0.5 mA/cm^2 after 2 min and

dx.doi.org/10.1021/am5021414 | ACS Appl. Mater. Interfaces 2014, 6, 9742–9750

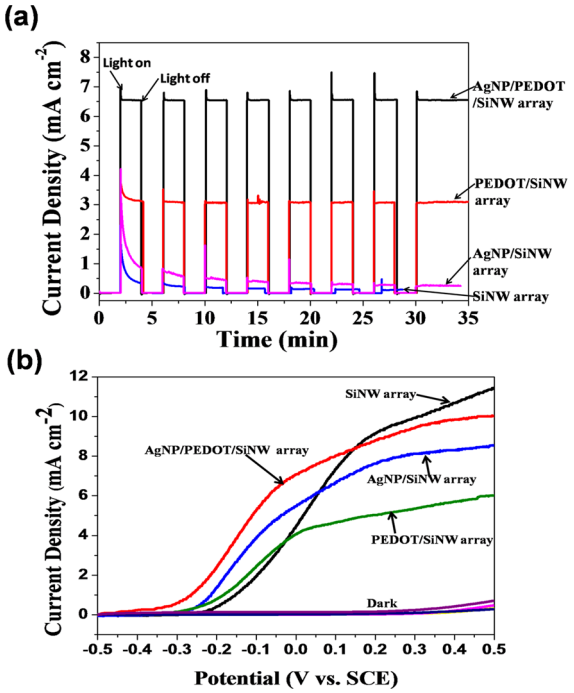

Figure 3. (a) Short-circuit photocurrent response of the different photoanodes. All currents were measured with three-electrode photoelectrolysis cells at zero applied potential (vs SCE) under irradiation with a xenon lamp with an intensity of 100 mW/cm^2. A water/methanol (v/v = 1:1) solution (PH = 1, adjusted with H_2SO_4) was used as the electrolyte and it was sufficiently saturated with N_2 before the measurement. (b) Typical current-potential characteristics of the different photoanodes in the dark and under illumination, collected at a scan rate of 50 mV/s from −0.5 to +0.5(V vs SCE).

10 min of irradiation, respectively. It is proposed that the continuous decay could be attributed to the gradual oxidation of the SiNW surface. In comparison to those two arrays, the PEDOT/SiNW arrays show steadier photoanodic current density (3.2 mA/cm^2) behavior; however, the photocurrent dropped slightly in the first 2 min of illumination. This might due to the carriers that accumulated on the surface of the photoanode before illumination, which increased the capacitance of the photoanode/electrolyte interface. Thus, at the beginning of illumination, the photocurrent was comparatively high as a result of the stack of the accumulated carriers and the photo-generated carriers produced under illumination. As the accumulated carriers were exhausted, PEDOT/SiNW arrays' photocurrent became steady, especially under continuous illumination (SI Figure S6). PEDOT/SiNW arrays' steady photocurrent reveals that PEDOT can be an effective protective layer for preventing photocorrosion of SiNW. Meanwhile, the suitable thickness of PEDOT coating can be achieved after 15 cycles of cyclic voltammetry,[23,24] which is feasible to protect the SiNWs from photocorrosion without interfering SiNWs' light absorption (SI S9). Moreover, the AgNPs/PEDOT/SiNW arrays achieved the strongest photocurrent density of 6.6 mA/cm^2 under the same conditions. As the applied potential is inadequate to trigger the reaction on the photoanode in dark condition, the current density was sharply decreased to only ∼0.01 mA/cm^2 when the light was turned off (Figure 3a).

The observation of the on−off switching of the photocurrent response reveals that the photocurrent of the AgNPs/PEDOT/SiNW array is nearly 2 times higher than that of the PEDOT/SiNW array. This enhancement of the photocurrent could be attributed to the enhanced photo-absorption arising from the efficient plasmon resonance between AgNPs and SiNWs, as discussed above; this may also be due to the resonant energy transfer between the AgNPs and the SiNWs arising from the overlap of the oscillator frequencies of the AgNP surface plasmon and semiconductor, which has been observed to increase the number of photo-excited carriers.[39] Furthermore, it is proposed that the fine-tuned conducting PEDOT layer can help to release the lattice mismatch between the AgNPs and SiNWs, which is favorable for high efficiency photo-generated carrier diffusion and stable photocatalysis in aqueous solutions. As shown in Figure 3b, the onset potential (the potential where the photocurrent density achieves 0.05 mA/cm^2) of H-SiNW, AgNPs/SiNW, PEDOT/SiNW, and AgNPs/PEDOT/SiNW arrays are −0.258 V, −0.306 V, −0.367V, and −0.491 V, respectively. This might be attributed to the modification layer of conductive polymer PEDOT which can facilitate the transfer of photo-generated holes from SiNWs to solution.[25,26] Meanwhile, the enhanced light-absorption caused by plasmonic AgNPs might also promote the production of photo-generated carriers.[27,28] These two factors can enhance the photocurrent, thus offering AgNPs/PEDOT/SiNW arrays the most negative onset potential.

The photoactivity of the planar Si with the AgNPs/PEDOT/Si wafer structure was also investigated under the same conditions to confirm the SiNWs' photocatalytic performance (SI S7). The results reveal that the photocurrent from the Si wafer is about 30 times weaker than that of the SiNW arrays, revealing that the main photocatalyst ability is due to the SiNW arrays and not the Si substrate.

The IPCE is a widely used parameter for the characterization of photoelectrodes. The IPCEs of four PEC cells with different SiNW arrays as photoanodes were measured to demonstrate the enhanced stability and improved photoelectric conversion efficiency of the AgNPs/PEDOT/SiNW structure (Figure 4a). In comparison to H-SiNW arrays, three modified SiNW arrays exhibited substantially enhanced IPCEs; among them, the AgNPs/PEDOT/SiNW arrays exhibited the highest IPCE of 42% at 510 nm. The PEDOT/SiNW arrays exhibited an IPCE of ∼25% at around 600 nm and then dropped gradually to ∼18% at 870 nm, while the AgNPs/SiNW arrays exhibited an IPCE of ∼37% centered at 630 nm. As shown in Figure 3a, the H-SiNW arrays and AgNPs/SiNW arrays are unstable in aqueous solutions since they are not coated by PEDOT; they were refreshed by HF before measurement at other wavelengths (SI S8); therefore, their photocurrents contain the currents raised from oxidation of Si. The results reveal that even with the oxidation current, the IPCE of AgNPs/SiNW is still lower than AgNPs/PEDOT/SiNW. It demonstrates that AgNPs/PEDOT/SiNW structure is stable and efficient.

Figure 4b shows the ratio of the IPCE obtained by the AgNPs/PEDOT/SiNW array and the PEDOT/SiNW array photoelectrodes as a function of source wavelength. The result shows that the IPCE ratio depends strongly on the source wavelength with the maximum value in the range from 350 nm to 450 nm. It should be noted that the UV−vis absorptions of the SiNWs and AgNPs also overlapped in this waveband (Figure 2b). The coincidence that the maximum of IPCE enhancement and UV−vis absorptions' overlapping appeared in the same waveband demonstrated that the efficient plasmonic resonance between AgNPs and SiNWs is the reason for the photocurrent enhancement of AgNPs/PEDOT/SiNW

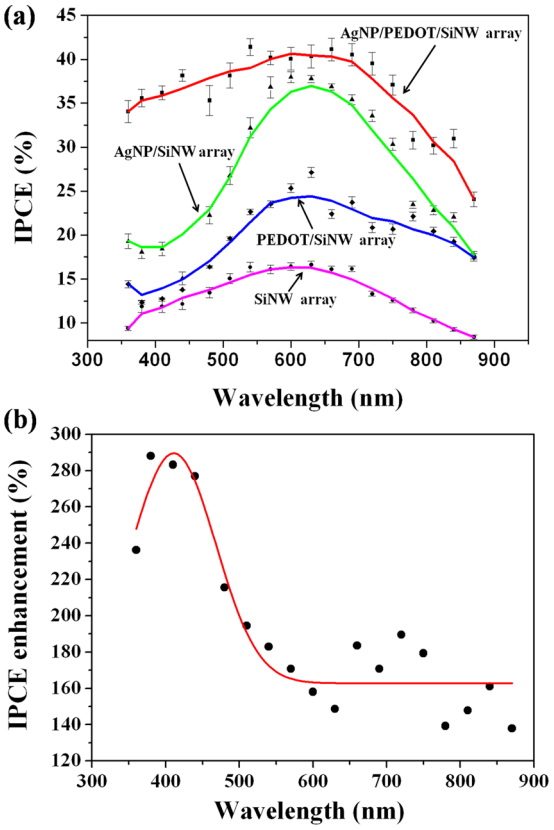

Figure 4. (a) IPCE spectra of the various photoanodes collected at the incident wavelength range from 360 to 870 nm at a potential of 0 V vs SCE. (b) (symbols) the ratio of IPCE obtained by AgNPs/PEDOT/SiNW arrays and PEDOT/SiNW arrays (IPCE for AgNPs/PEDOT/SiNW divided by that for PEDOT/SiNW) as a function of excitation wavelength. Solid curve is a nonlinear curve fit to the measurement points.

array.[28,39,50,53] In addition, the electromagnetic responses of the composite photocatalysts that fabricated by decorating semiconductors with plasmonic metal nanoparticles have been investigated with 3-D finite difference time domain (FDTD) simulation in previously studies.[54,55] The result reveals that the electromagnetic field intensity between the plasmonic metal nanoparticles and semiconductors could be enhanced dramatically, which agrees well with the enhanced photocurrent in our work.

Based on the photocurrent and IPCE measurements, it can be concluded that the efficient and stable photocatalytic activity of AgNPs/PEDOT/SiNW arrays may be due to the following reasons: (1) the nanoscale PEDOT layer can efficiently prevent photocorrosion of the SiNW; (2) the conducting PEDOT layer is efficient as a surface plasmon resonator between AgNPs and SiNWs; (3) soft PEDOT layer helps firmly decorate AgNPs onto SiNW surfaces and prevents surface recombination centres that arise from surface lattice mismatch.[43] Consequently, the visible light photoanode that was synthesized by first stabilizing the SiNW arrays with PEDOT followed by activation the stable Si/PEDOT core/shell nanowire arrays with plasmonic AgNPs exhibits a steady IPCE enhancement. Table 1 lists the IPCEs of the representative photoanodes for PEC hydrogen production; our result is among the best reported for photocatalyzed hydrogen production systems.[44−49]

In Figure 5, solar hydrogen evolution rate in the PEC cell is shown to be 36.05 μmol/(cm^2·h) in a water/methanol (v/v = 1/1) solution (pH = 1, adjusted with H_2SO_4) under 100 mW cm^{-2} illumination from a xenon lamp with no external potential

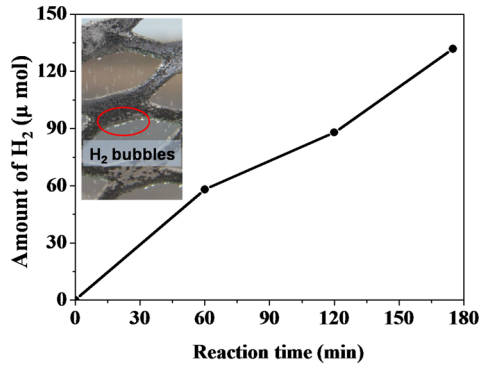

Figure 5. Plot of hydrogen evolution calculated per cm^2 as a function of time with AgNPs/PEDOT/SiNW arrays as the photoanode and Pt mesh as the cathode. The experiment was performed in a two-electrode system with a water/methanol (v/v = 1:1) solution (pH = 1, adjusted with H_2SO_4) under 100 mW cm^{-2} illumination from a xenon lamp with no external potential applied on the working electrode. Inset: photographed H_2 bubbles produced on the Pt mesh.

Table 1. Summary of the IPCEs of the Representative Photoanodes for PEC Hydrogen Production

				IPCE of different wavelength					
	electrode	electrolyte	measurement method	400 nm	500 nm	600 nm	700 nm	800 nm	wavelength range (IPCE > 30%)
this work[a]	AgNPs/PEDOT/SiNW	water/methanol (v/v = 1/1) 0.05 M H_2SO_4	3-electrode system, 0 V vs SCE	35%	37%	40%	38%	33%	360−840 nm
ref 44[a]	ZnTAPc/SiNW	0.8 M KI/H_2SO_4 (pH = 3)	3-electrode system, 0 V vs SCE	4%	7%	12%	9%	6%	
ref 45[a]	CdS−ZnO−ZnO−CdSe	0.25 M Na_2S and 0.35 M Na_2SO_3	3-electrode system, 0 V vs Ag/AgCl	45%	43%	40%			360−640 nm
ref 46[b]	AgNP/WO_3 film	1 M H_2SO_4	3-electrode system, 1.5 V/RHE	70%	0				400−440 nm
ref 47[b]	AuNPs/Fe_2O_3/SiNW	1 M NaOH	3-electrode system, 0 V/Pt electrode	3%	5%	8%	12%	15%	
ref 48[a]	ZnS QDs/ZnO nanowire arrays	0.5 M Na_2S and K_2SO_3 (pH = 11)	3-electrode system, 0.5 V vs Ag/AgCl	12%	1%				
ref 49[a]	CdS−H:TiO_2 nanowire arrays	0.25 M Na_2S and 0.35 M Na_2SO_3 (pH = 11.5)	3-electrode system, 0.5 V/RHE	70%	45%	0			360−520 nm

[a]PEC system with sacrificial electron donor. [b]PEC system without sacrificial electron donor.

dx.doi.org/10.1021/am5021414 | ACS Appl. Mater. Interfaces 2014, 6, 9742−9750

applied on the working electrode. The experiment was carried out in a two-electrode system; AgNPs/PEDOT/SiNW arrays were used as the work electrode, meanwhile, the counter electrode and reference electrode were joined together. The generated H_2 was characterized by GC analysis (14B Shimadzu) using nitrogen as the carrier gas with a molecular sieve column (5 Å; 30 m × 0.53 mm) and a thermal conductivity detector. The amount of hydrogen produced was measured every 60 min. During the entire experiment, the H_2 evolution rate did not decrease and the electrode showed good stability. In the two-electrode system and without an external potential, the solar-to-chemical energy conversion efficiency of the PEC cell could be calculated as the chemical energy of the produced H_2 divided by the solar energy input.[51] As clear energy source, hydrogen is widely used as fuel to react with oxygen and produce water. Based on this practical application and the stable solar hydrogen evolution rate of 36.05 μmol/(cm^2·h), it was calculated that the photoanode can support an energy density of 36.05/3600 μmol/(cm^2·s) × 286 kJ/mol = 2.86 mW·cm^{-2} (the combustion enthalpy of H_2 is −286 kJ/mol).[52] As the light applied energy is 100 mW cm^{-2}, the solar-to-chemical energy conversion efficiency of the PEC system can reach up to 2.86%. It is expected that this conversion efficiency may be further improved to 5% through controlling the pattern of the SiNW arrays and reducing the loss of hydrogen during collection.

CONCLUSIONS

In conclusion, this study demonstrates a new strategy for designing stable visible light photoanodes for PEC solar hydrogen generation. This method involves coating a nanoscale conducting polymer layer on narrow-band-gap semiconductor NWs to stabilize their surfaces, and then activate its visible light absorption with plasmonic metal nanoparticles. As an example, the AgNPs/PEDOT/SiNW array photoanode was utilized for solar hydrogen generation from a water/methanol mixture in the PEC cell with a solar-to-chemical energy conversion efficiency of 2.86% and a steady IPCE of ∼35−42% across the visible region from 360 to 870 nm. The presented strategy of conductive polymer protection and plasmonic metal nanoparticles activation is expected to offer improved corrosion protection and solar energy harvesting for other narrow-band-gap semiconductors employed in visible light photoelectrochemical and photoelectric conversion applications.

ASSOCIATED CONTENT

Supporting Information

Synthesis procedures of SiNW arrays, electro-polymerization of PEDOT, IR spectrum of PEDOT modified SiNWs, synthesis procedures of AgNPs/SiNW arrays, hydrogen production measurement, photoelectrochemical measurements of SiNW arrays and planar Si based photocatalysts, IPCE measurement of the photocatalysts, UV−vis asorption spectra of PEDOT film. This material is available free of charge via the Internet at http://pubs.acs.org.

AUTHOR INFORMATION

Corresponding Author

*Email: xhzhang@mail.ipc.ac.cn.

Author Contributions

‖C.D. and H.W. contributed equally to this work.

Funding

This work was supported by the National Basic Research Program of China (973 Program) (Grant Nos. 2012CB932400, 2010CB934500), the National Natural Science Foundation of China (Grant Nos. 51172246, 51373188), the Major Research Plan of the National Natural Science Foundation of China (Grant No. 91333208)

Notes

The authors declare no competing financial interest.

REFERENCES

(1) Reece, S. Y.; Hamel, J. A.; Sung, K.; Jarvi, T. D.; Esswein, A. J.; Pijpers, J. J. H.; Nocera, D. G. Wireless Solar Water Splitting Using Silicon-based Semiconductors and Earth-Abundant Catalysts. *Science* **2011**, *334*, 645−648.

(2) Han, Z.; Qiu, F.; Eisenberg, R.; Holland, P. L.; Krauss, T. D. Robust Photogeneration of H_2 in Water Using Semiconductor Nanocrystals and a Nickel Catalyst. *Science* **2012**, *338*, 1321−1324.

(3) Fujishima, A.; Honda, K. Photolysis−Decomposition of Water at the Surface of an Irradiated Semiconductor. *Nature* **1972**, *238*, 37−38.

(4) Walter, M. G.; Warren, E. L.; McKone, J. R.; Boettcher, S. W.; Mi, Q.; Santori, E. A.; Lewis, N. S. Solar Water Splitting Cells. *Chem. Rev.* **2010**, *110*, 6446−6473.

(5) Maeda, K.; Higashi, M.; Lu, D.; Abe, R.; Domen, K. Efficient Nonsacrificial Water Splitting through Two-Step Photoexcitation by Visible Light Using a Modified Oxynitride as a Hydrogen Evolution Photocatalyst. *J. Am. Chem. Soc.* **2010**, *132*, 5858−5868.

(6) Chen, X.; Shen, S.; Guo, L.; Mao, S. S. Semiconductor-based Photocatalytic Hydrogen Generation. *Chem. Rev.* **2010**, *110*, 6503−6570.

(7) Yi, Z.; Ye, J.; Kikugawa, N.; Kako, T.; Ouyang, S.; Stuart-Williams, H.; Yang, H.; Cao, J.; Luo, W.; Li, Z.; Liu, Y.; Withers, R. L. An Orthophosphate Semiconductor with Photooxidation Properties under Visible-Light Irradiation. *Nat. Mater.* **2010**, *9*, 559−564.

(8) Chen, X.; Liu, L.; Yu, P. Y.; Mao, S. S. Increasing Solar Absorption for Photocatalysis with Black Hydrogenated Titanium Dioxide Nanocrystals. *Science* **2011**, *331*, 746−750.

(9) Tong, H.; Ouyang, S.; Bi, Y.; Umezawa, N.; Oshikiri, M.; Ye, J. Nano-photocatalytic Materials: Possibilities and Challenges. *Adv. Mater.* **2012**, *24*, 229−251.

(10) Zhou, W. J.; Liu, H.; Wang, J. Y.; Liu, D.; Du, G.J.; Cui, J. J. Ag_2O/TiO_2 Nanobelts Heterostructure with Enhanced Ultraviolet and Visible Photocatalytic Activity. *ACS Appl. Mater. Interfaces* **2010**, *2*, 2385−2392.

(11) Xie, Y.; Ghafar, A.; Seung, H. Y.; Sung, O. C. Sonication-assisted Synthesis of CdS Quantum-Dot-Sensitized TiO_2 Nanotube Arrays with Enhanced Photoelectrochemical and Photocatalytic Activity. *ACS Appl. Mater. Interfaces* **2010**, *2*, 2910−2914.

(12) Lü, X.; Huang, F.; Wu, J.; Ding, S.; Xu, F. Intelligent Hydrated-Sulfate Template Assisted Preparation of Nanoporous TiO_2 Spheres and Their Visible-Light Application. *ACS Appl. Mater. Interfaces* **2011**, *3*, 566−572.

(13) Shalom, M.; Hod, I.; Tachan, Z.; Buhbut, S.; Tirosh, S.; Zaban, A. Quantum Dot Based Anode and Cathode for High Voltage Tandem Photo-electrochemical Solar Cell. *Energy Environ. Sci.* **2011**, *4*, 1874−1878.

(14) Dotan, H.; Sivula, K.; Gratzel, M.; Rothschild, A.; Warren, S. C. Probing the Photoelectrochemical Properties of Hematite (α-Fe_2O_3) Electrodes Using Hydrogen Peroxide as a Hole Scavenger. *Energy Environ. Sci.* **2011**, *4*, 958−964.

(15) Wang, P.; Wang, D. G.; Lin, J.; Li, X. L.; Peng, C.; Gao, X. Y.; Huang, Q.; Wang, J. Q.; Xu, H. J.; Fan, C. H. Lattice Defect-Enhanced Hydrogen Production in Nanostructured Hematite-based Photoelectrochemical Device. *ACS Appl. Mater. Interfaces* **2012**, *4*, 2295−2302.

(16) Wang, D. G.; Zhang, Y. Y.; Wang, J. Q.; Peng, C.; Huang, Q.; Su, S.; Wang, L. H.; Huang, W.; Fan, C. H. Template-free Synthesis of Hematite Photoanodes with Nanostructured ATO Conductive

Underlayer for PEC Water Splitting. *ACS Appl. Mater. Interfaces* **2014**, *6*, 36−40.
(17) Seiji, K.; Toshiyuki, A. A Novel Example of Molecular Hydrogen Generation from Formic Acid at Visible-Light-Responsive Photocatalyst. *ACS Appl. Mater. Interfaces* **2009**, *1*, 2707−2710.
(18) Sasaki, Y.; Kato, H.; Kudo, A. $[Co(bpy)_3]^{3+/2+}$ and $[Co(phen)_3]^{3+/2+}$ Electron Mediators for Overall Water Splitting under Sunlight Irradiation Using Z-scheme Photocatalyst System. *J. Am. Chem. Soc.* **2013**, *135*, 5441−5449.
(19) Shimura, K.; Yoshida, H. Heterogeneous Photocatalytic Hydrogen Production from Water and Biomass Derivatives. *Energy Environ. Sci.* **2011**, *4*, 2467−2481.
(20) Grimes, C. A.; Varghese, O. K.; Ranjan, S. *Light, Water, Hydrogen The Solar Generation of Hydrogen by Water Photoelectrolysis*; Springer 2008.
(21) Chen, Y. W.; Prange, J. D.; Duhnen, S.; Park, Y.; Gunji, M.; Chidsey, C. E. D.; Mclntyre, P. C. Atomic Layer-Deposited Tunnel Oxide Stabilizes Silicon Photoanodes for Water Oxidation. *Nat. Mater.* **2011**, *10*, 539−544.
(22) Wang, X.; Peng, K. Q.; Pan, X. J.; Chen, X.; Yang, Y.; Li, L.; Meng, X. M.; Zhang, W. J.; Lee, S. T. High-Performance Silicon Nanowire Array Photoelectrochemical Solar Cells through Surface Passivation and Modification. *Angew. Chem. Int. Ed.* **2011**, *50*, 9861−9865.
(23) Liu, Z.; Wang, H.; Ou, X. M.; Lee, C. S.; Zhang, X. H. Si/poly-CuTAPc Coaxial Core−Shell Nanowire Array as Enhanced Visible-light Pohotocatalyst for Hydrogen Production. *Chem. Commun.* **2012**, *48*, 2815−2817.
(24) Yang, T.; Wang, H.; Ou, X. M.; Lee, C. S.; Zhang, X. H. Iodine-doped-poly(3,4-ethylenedioxythiophene)-modified Si Nanowire 1D Core-Shell Arrays as an Efficient Photocatalyst for Solar Hydrogen Generation. *Adv. Mater.* **2012**, *24*, 6199−6203.
(25) Shiu, S. C.; Chao, J. J.; Hung, S. C.; Yeh, C. L.; Lin, C. F. Morphology Dependence of Silicon Nanowire/Poly(3,4-ethylenedioxythiophene): Poly(styrenesulfonate) Heterojunction Solar Cells. *Chem. Mater.* **2010**, *22*, 3108−3113.
(26) Jeong, S.; Garnett, E. C.; Wang, S.; Yu, Z.; Fan, S.; Brongersma, M. L.; McGehee, M. D.; Cui, Y. Hybrid Silicon Nanocone−Polymer Solar Cells. *Nano Lett.* **2012**, *12*, 2971−2976.
(27) Schuller, J. A.; Barnard, E. S.; Cai, W.; Jun, Y. C.; White, J. S.; Brongersma, M. L. Plasmonics for Extreme Light Concentration and Manipulation. *Nat. Mater.* **2010**, *9*, 193−204.
(28) Warren, S. C.; Thimsen, E. Plasmonic Solar Water Splitting. *Energy Environ. Sci.* **2012**, *5*, 5133−5146.
(29) Pan, C.; Xu, J.; Wang, Y.; Li, D.; Zhu, Y. Dramatic Activity of $C_3N_4/BiPO_4$ Photocatalyst with Core/Shell Structure Formed by Self-assembly. *Adv. Funct. Mater.* **2012**, *22*, 1518−1524.
(30) Qu, Y.; Cheng, R.; Su, Q.; Duan, X. Plasmonic Enhancements of Photocatalytic Activity of Pt/n-Si/Ag Photodiodes Using Au/Ag Core/Shell Nanorods. *J. Am. Chem. Soc.* **2011**, *133*, 16730−16733.
(31) Ahonen, H. J.; Lukkari, J.; Kankare, J. N- and P-doped Poly(3,4-ethylenedioxythiophene): Two Electronically Conducting States of the Polymer. *Macromolecules* **2000**, *33*, 6787−6793.
(32) Groenendaal, L.; Jonas, F.; Freitag, D.; Pielartzik, H.; Reynolds, J. R. Poly(3,4-ethylenedioxythiophene) and Its Derivatives: Past, Present, and Future. *Adv. Mater.* **2000**, *12*, 481−494.
(33) Peng, K. Q.; Lee, S. T. Silicon Nanowires for Photovoltaic Solar Energy Conversion. *Adv. Mater.* **2011**, *23*, 198−215.
(34) Shao, M. W.; Cheng, L.; Zhang, X. H.; Ma, D. D. D.; Lee, S. T. Excellent Photocatalysis of HF-Treated Silicon Nanowires. *J. Am. Chem. Soc.* **2009**, *131*, 17738−17739.
(35) Shi, J.; Hara, Y.; Sun, C.; Anderson, M. A.; Wang, X. Three-Dimensional High-Density Hierarchical Nanowire Architecture for High-Performance Photoelectrochemical Electrodes. *Nano Lett.* **2011**, *11*, 3413−3419.
(36) Peng, K.Q.; Lu, A.; Zhang, R.; Lee, S. T. Motility of Metal Nanoparticles in Silicon and Induced Anisotropic Silicon Etching. *Adv. Funct. Mate.* **2008**, *18*, 3026−3035.
(37) Asami, R.; Atobe, M.; Fuchigami, T. Electropolymerization of an Immiscible Monomer in Aqueous Electrolytes Using Acoustic Emulsification. *J. Am. Chem. Soc.* **2005**, *127*, 13160−13161.
(38) El-Sayed, M. A. Some Interesting Properties of Metals Confined in Time and Nanometer Space of Different Shapes. *Acc. Chem. Res.* **2001**, *34*, 257−264.
(39) Ingram, D. B.; Linic, S. Water Splitting on Composite Plasmonic-Metal /Semiconductor Photoelectrodes: Evidence for Selective Plasmon-Induced Formation of Charge Carriers near the Semiconductor Surface. *J. Am. Chem. Soc.* **2011**, *133*, 5202−5205.
(40) Thimsen, E.; Formal, F. L.; Gratzel, M.; Warren, S. C. Influence of Plasmonic Au Nanoparticles on the Photoactivity of Fe_2O_3 Electrodes for Water Splitting. *Nano Lett.* **2011**, *11*, 35−43.
(41) Xu, H.; Li, H. M.; Xia, J. X.; Yin, S.; Luo, Z. J.; Liu, L.; Xu, L. One-Pot Synthesis of Visible-Light-Driven Plasmonic Photocatalyst Ag/AgCl in Ionic Liquid. *ACS Appl. Mater. Interfaces* **2011**, *3*, 22−29.
(42) Cushing, S. K.; Li, J.; Meng, F.; Senty, T. R.; Suri, S.; Zhi, M.; Li, M.; Bristow, A. D.; Wu, N. Photocatalytic Activity Enhanced by Plasmonic Resonant Energy Transfer from Metal to Semiconductor. *J. Am. Chem. Soc.* **2012**, *134*, 15033−15041.
(43) Han, X. M.; Wang, H.; Ou, X. M.; Zhang, X. H. Highly Sensitive, Reproducible, and Stable SERS Sensors Based on Well-controlled Silver Nanoparticle-Decorated Silicon Nanowire Building Blocks. *J. Mater. Chem.* **2012**, *22*, 14127−14132.
(44) Liu, Z.; Wang, H.; Ou, X. M.; Lee, C. S.; Li, F.; Zhang, X. H. A Silicon/Zinc 2,9,16,23-Tetraamino-Phthalocyanine Coaxial Core−Shell Nanowire Array as an Efficient Solar Hydrogen Generation Photocatalyst. *Nanotechnology* **2012**, *23*, 175401.
(45) Wang, G.; Yang, X.; Qian, F.; Zhang, J. Z.; Li, Y. Double-Sided CdS and CdSe Quantum Dot Co-sensitized ZnO Nanowire Arrays for Photoelectrochemical Hydrogen Generation. *Nano Lett.* **2010**, *10*, 1088−1092.
(46) Solarska, R.; Królikowska, A.; Augustyński, J. Silver Nanoparticle Induced Photocurrent Enhancement at WO_3 Photoanodes. *Angew. Chem. Int. Ed.* **2010**, *49*, 7980−7983.
(47) Wang, X.; Peng, K. Q.; Hu, Y.; Zhang, F. Q.; Hu, B.; Li, L.; Wang, M.; Meng, X. M.; Lee, S. T. Silicon/Hematite Core/Shell Nanowire Array Decorated with Gold Nanoparticles for Unbiased Solar Water Oxidation. *Nano Lett.* **2014**, *14*, 18−23.
(48) Chen, H. M.; Chen, C. K.; Liu, R. S.; Wu, C. C.; Chang, W. S.; Chen, K. H.; Chan, T. S.; Lee, J. F.; Tsai, D. P. A New Approach to Solar Hydrogen Production: A ZnO−ZnS Solid Solution Nanowire Array Photoanode. *Adv. Energy Mater.* **2011**, *1*, 742−747.
(49) Wang, H.; Wang, G.; Ling, Y.; Lepert, M.; Wang, C.; Zhang, J. Z.; Li, Y. Photoelectrochemical Study of Oxygen Deficient TiO_2 Nanowire Arrays with CdS Quantum Dot Sensitization. *Nanoscale* **2012**, *4*, 1463−1466.
(50) Zhang, Z.; Zhang, L.; Hedhili, M. N.; Zhang, H.; Wang, P. Plasmonic Gold Nanocrystals Coupled with Photonic Crystal Seamlessly on TiO_2 Nanotube Photoelectrodes for Efficient Visible Light Photoelectrochemical Water Splitting. *Nano Lett.* **2013**, *13*, 14−20.
(51) Chen, Z. B.; Jaramillo, T. F.; Deutsch, T. G.; Kleiman-Shwarsctein, A.; Forman, A. J.; Gaillard, N.; Garland, R.; Takanabe, K.; Heske, C.; Sunkara, M.; McFarland, E. W.; Domen, K.; Miller, E. L.; Turner, J. A.; Dinh, H. N. Accelerating Materials Development for Photoelectrochemical Hydrogen Production: Standards for Methods, Definitions, and Reporting Protocols. *J. Mater. Res.* **2010**, *25*, 3−16.
(52) Committee on Alternatives and Strategies for Future Hydrogen Production and Use, National Research Council, National Academy of Engineering. *The Hydrogen Economy: Opportunities, Costs, Barriers, and R&D Needs*; National Academies Press: Washington, DC, 2004.
(53) Pu, Y. C.; Wang, G.; Chang, K. D.; Ling, Y.; Lin, Y. K.; Fitzmorris, B. C.; Liu, C. M.; Lu, X.; Tong, Y.; Zhang, J. Z.; Hsu, Y. J.; Li, Y. Au Nanostructure-Decorated TiO_2 Nanowires Exhibiting Photoactivity Across Entire UV−Visible Region for Photoelectrochemical Water Splitting. *Nano Lett.* **2013**, *13*, 3817−3823.

(54) Liu, Z.; Hou, W.; Pavaskar, P.; Aykol, M.; Cronin, S. B. Plasmon Resonant Enhancement of Photocatalytic Water Splitting Under Visible Illumination. *Nano Lett.* **2011**, *11*, 1111−1116.
(55) Brittman, S.; Gao, H.; Garnett, E. C.; Yang, P. Absorption of Light in a Single-Nanowire Silicon Solar Cell Decorated with an Octahedral Silver Nanocrystal. *Nano Lett.* **2011**, *11*, 5189−5195.